XMM Newton in the era of observational cosmology

Richard Lieu
University of Alabama, Huntsville

J. Mittaz, N. Werner, M. Bonamente, J.S. Kaastra

- Region: 1.5-3.1 arcmin, away from cooling core
- Fit to 1.5-7 keV (except ROSAT, fit 1.5-2 keV)
- KT = 5.9+- 0.1 keV, A=0.34+-0.02
- MOS EA at low energy soon to be revised to match PN excess

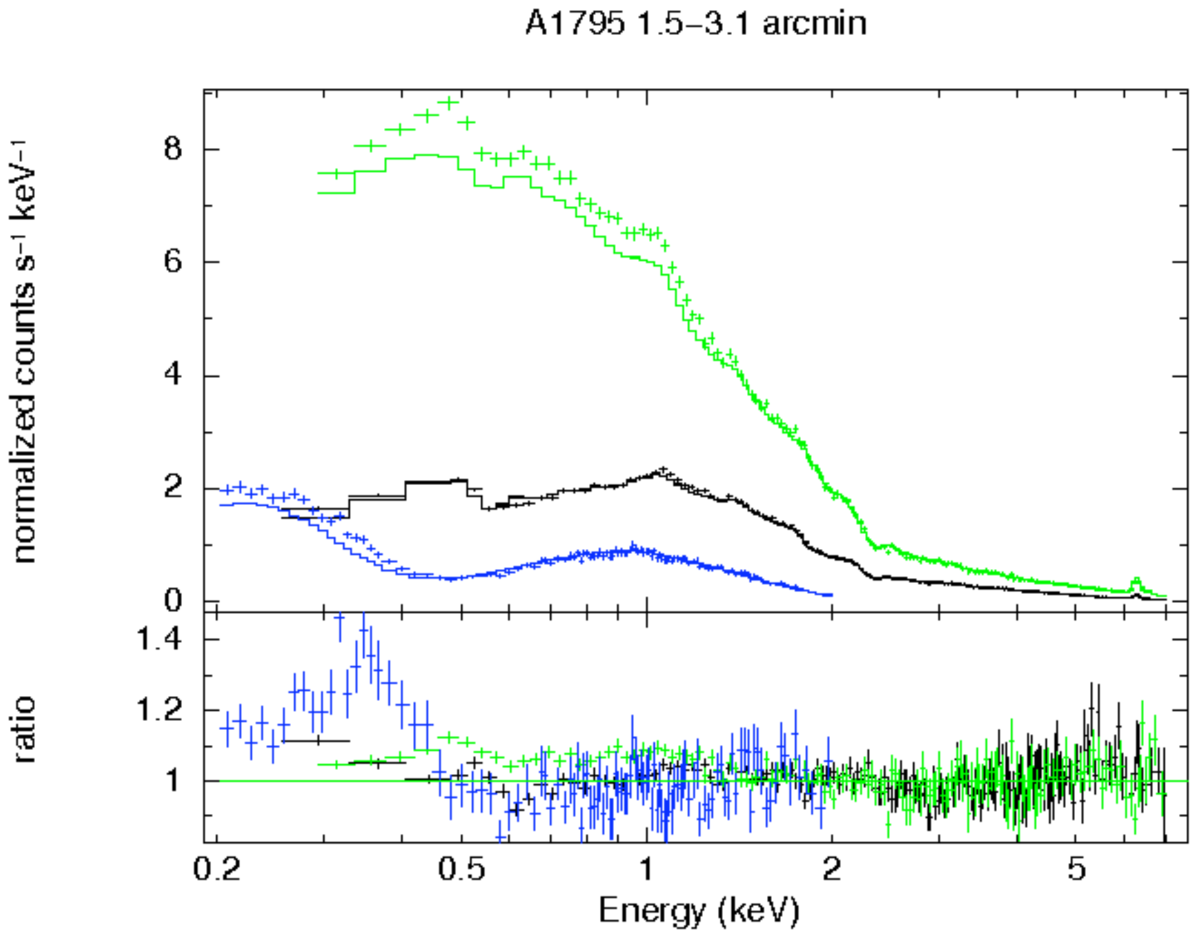

- Region: 0.5-1.5 arcmin, away from cooling core
- Fit to 1.5-7 keV (except ROSAT, fit to 1.5-2 keV), acceptable fit
- Normalizations free among datasets

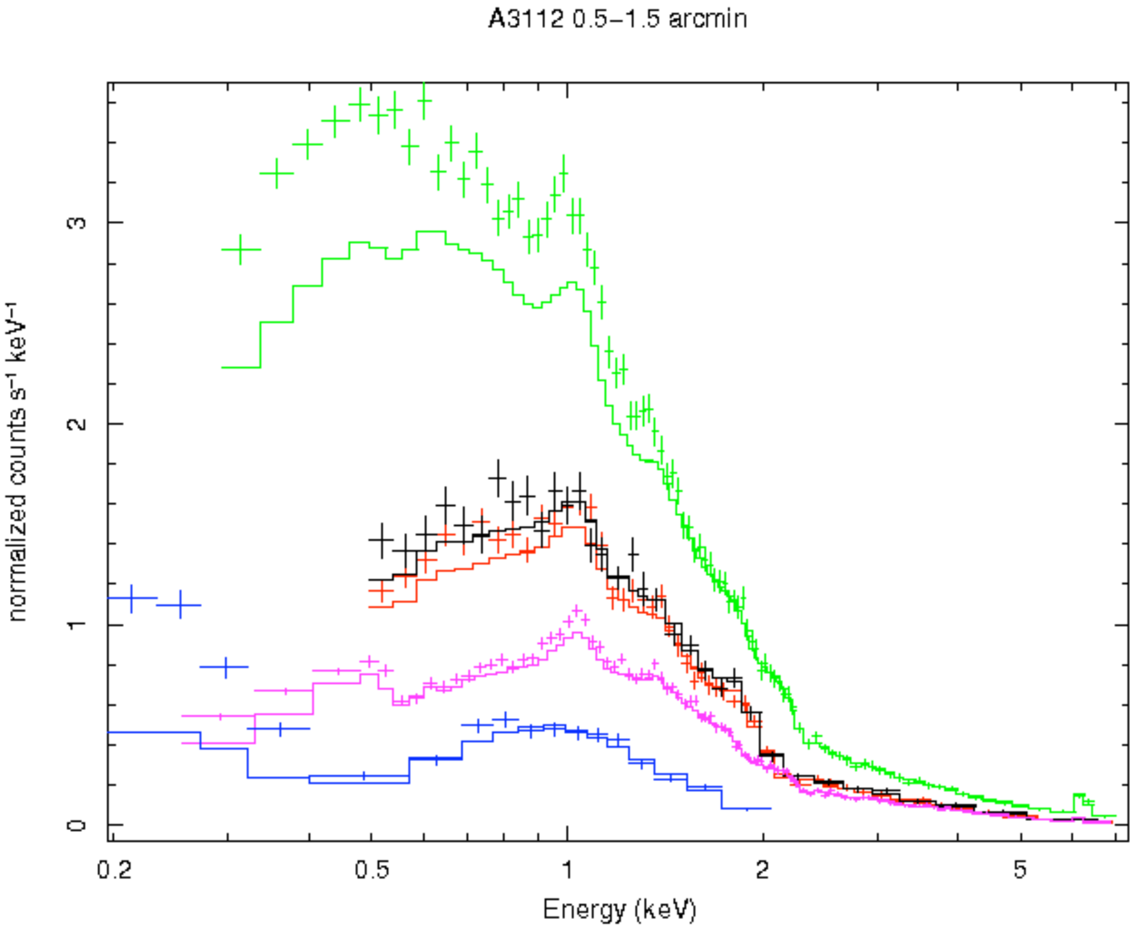

Note for A3112, cluster soft excess is not a background effect

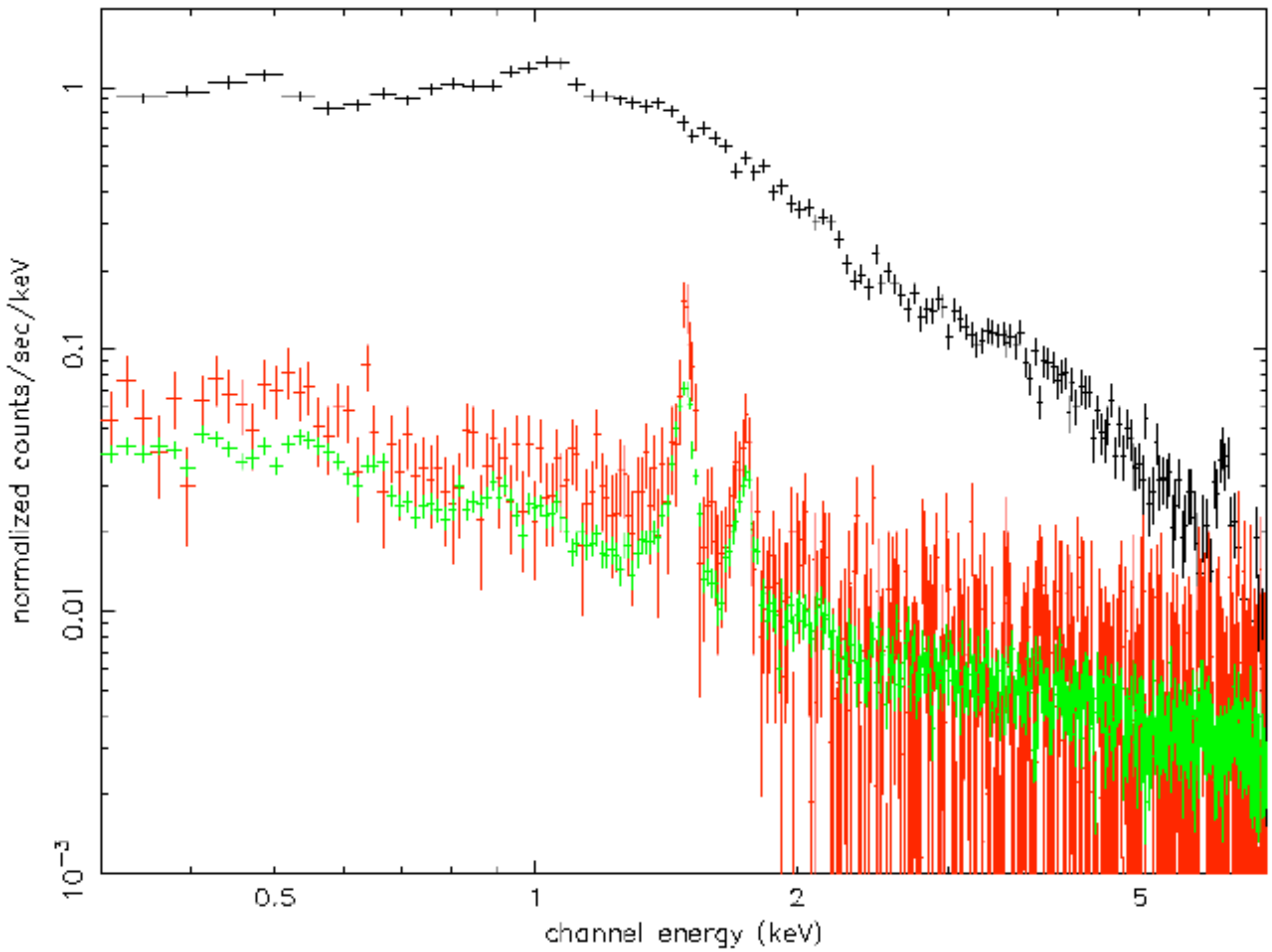

Physical constraints on the model

For intracluster origin of the WHIM

$$P_{warm} = P_{hot} \rightarrow n_w = (n_h / 10^{-3} cm^{-3}) \left(\frac{T_h}{T_w} \right)$$

If we take $T_h = 10 T_w, n_w > 10^{-2} cm^{-3}$

Radiative cooling time is important

$$\tau = 6 \times 10^9 (T / 10^6 K)^{0.5} (n_w / 10^{-3} cm^{-3})^{-1} yrs$$

For $T_w \sim 10^6 K, n_w > 10^{-2} cm^{-3}$ $\tau < 6 \times 10^8 \, years$

WHAT SUSTAINS THE WARM GAS AGAINST SUCH RAPID RADIATIVE COOLING?

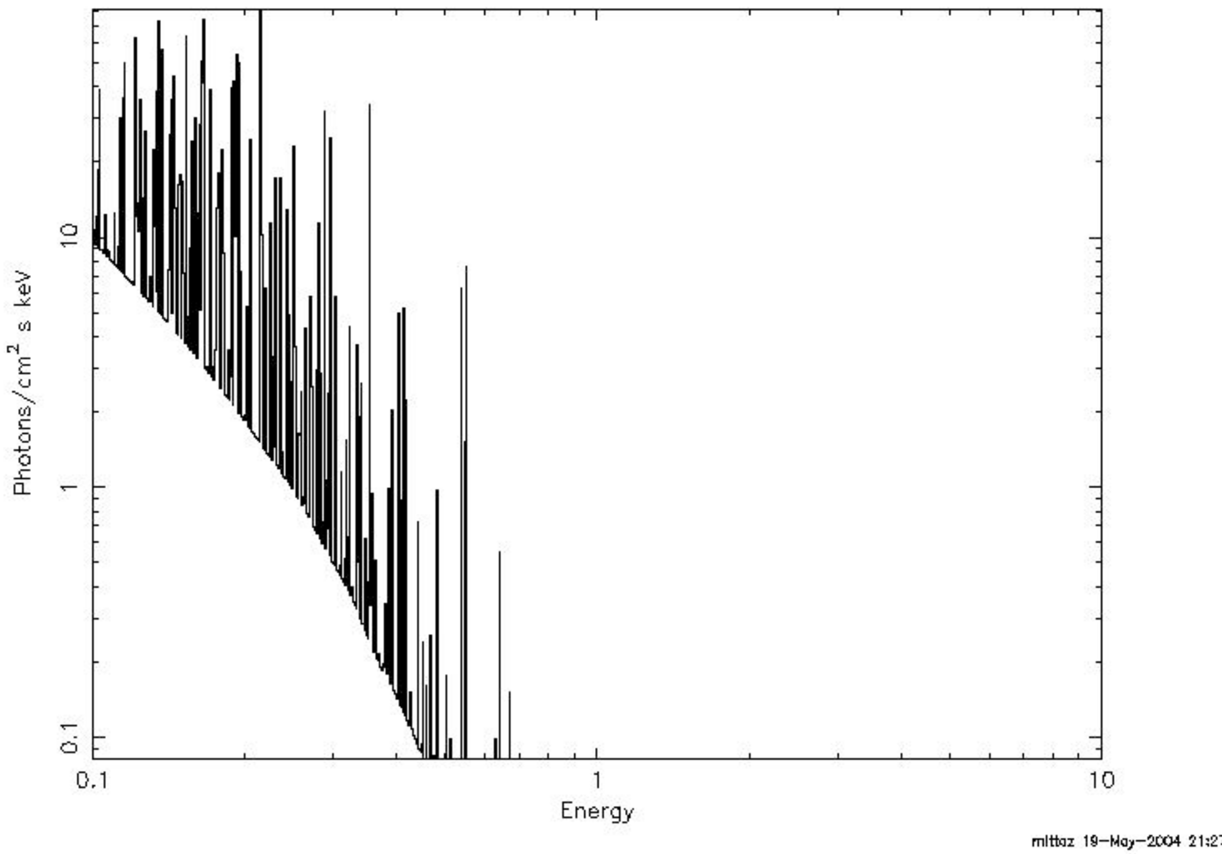

Thermal (mekal) model kT $\approx 10^6 K$

Non-thermal interpretation of the cluster soft excess

Hwang, C.-Y., 1997, Science, 278, 191
Ensslin, T.A. & Biermann, P.L., 1998, A&A, 330, 20
Sarazin, C.L. & Lieu, R., 1998, ApJ, 494, L177

Proposed the origin of the cluster soft excess emission as due to inverse-Compton scattering between intracluster cosmic rays (relativistic electrons with Lorentz factors of a few hundred) and the cosmic microwave background

HOW LARGE A COSMIC-RAY (CR) POPULATION DO WE NEED TO ACCOUNT FOR THE SOFT EXCESS BRIGHTNESS?

NB. Center can be e+/e- pairs, but outside has to be CR's from supernova events.

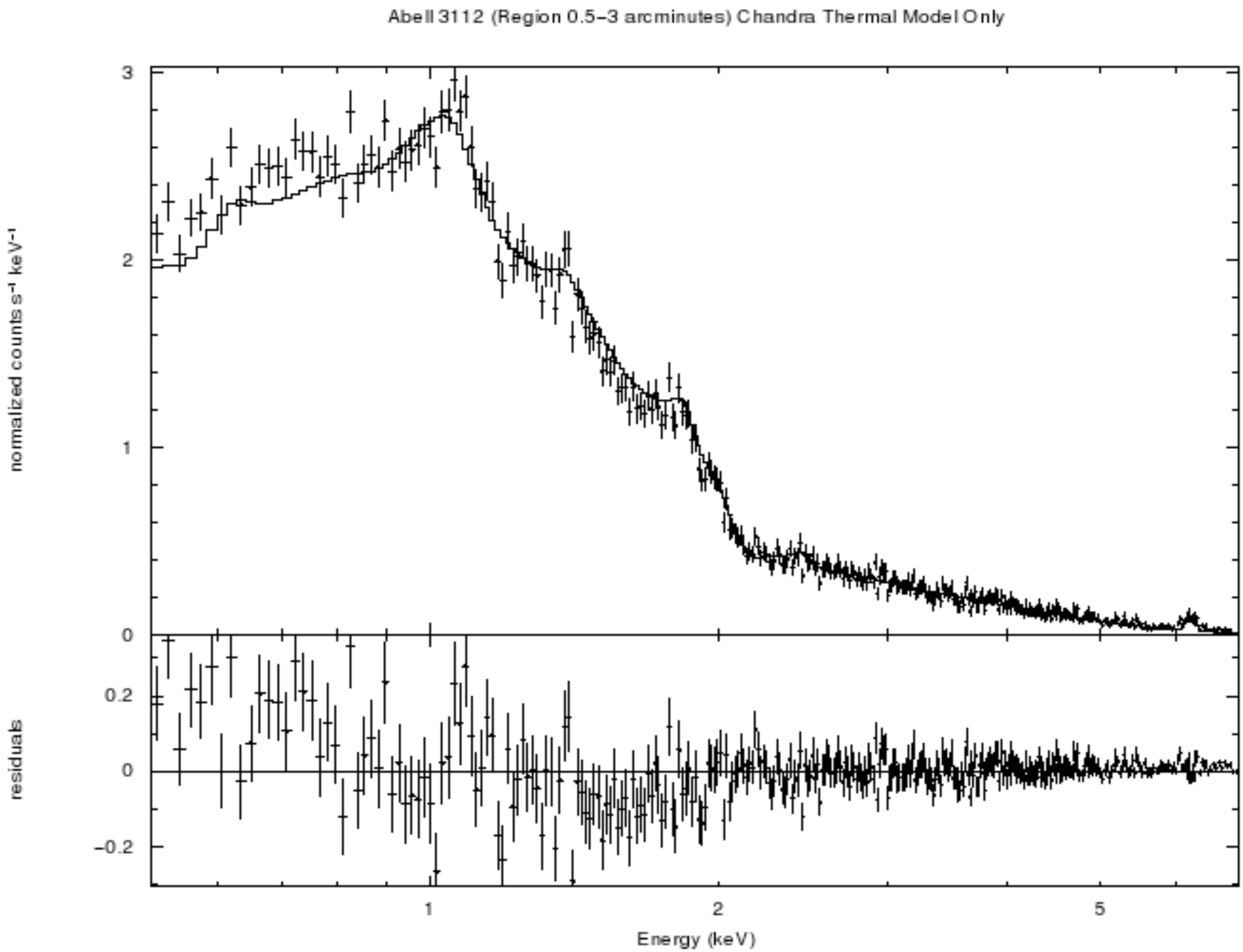
Abell 3112 (Region 0.5–3 arcminutes) Chandra Thermal Model Only
normalized counts s⁻¹ keV⁻¹
residuals
Energy (keV)
3
2
1
0
0.2
0
−0.2
1
2
5

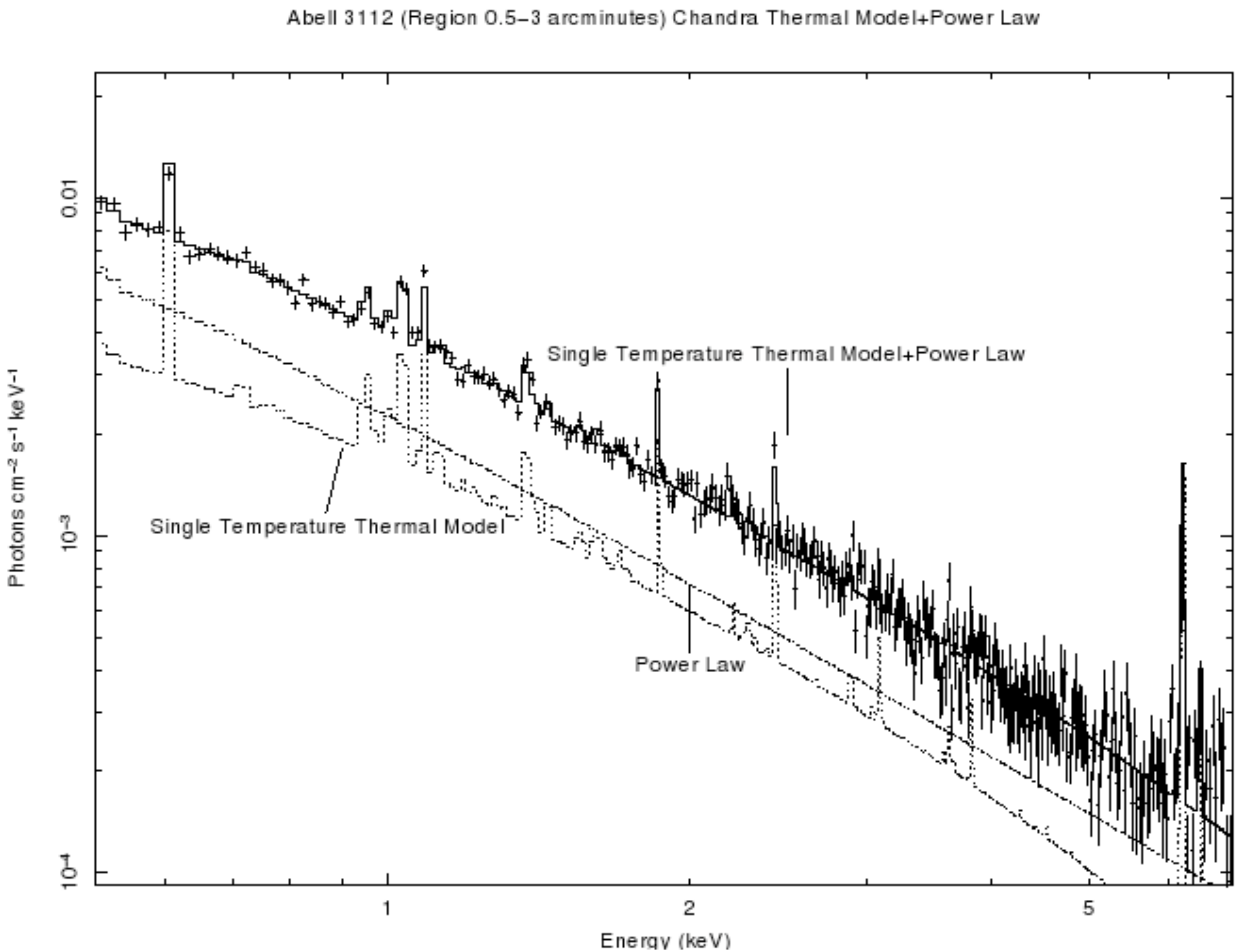

Abell 3112 (Region 0.5-3 arcminutes) Chandra Thermal Model+Power Law
Single Temperature Thermal Model+Power Law
Single Temperature Thermal Model
Power Law
Photons cm⁻² s⁻¹ keV⁻¹
0.01
10⁻³
10⁻⁴
1
2
5
Energy (keV)

Suzaku data of Abell S1101 central 3'-8' (Werner et al 2007 A & A in press)

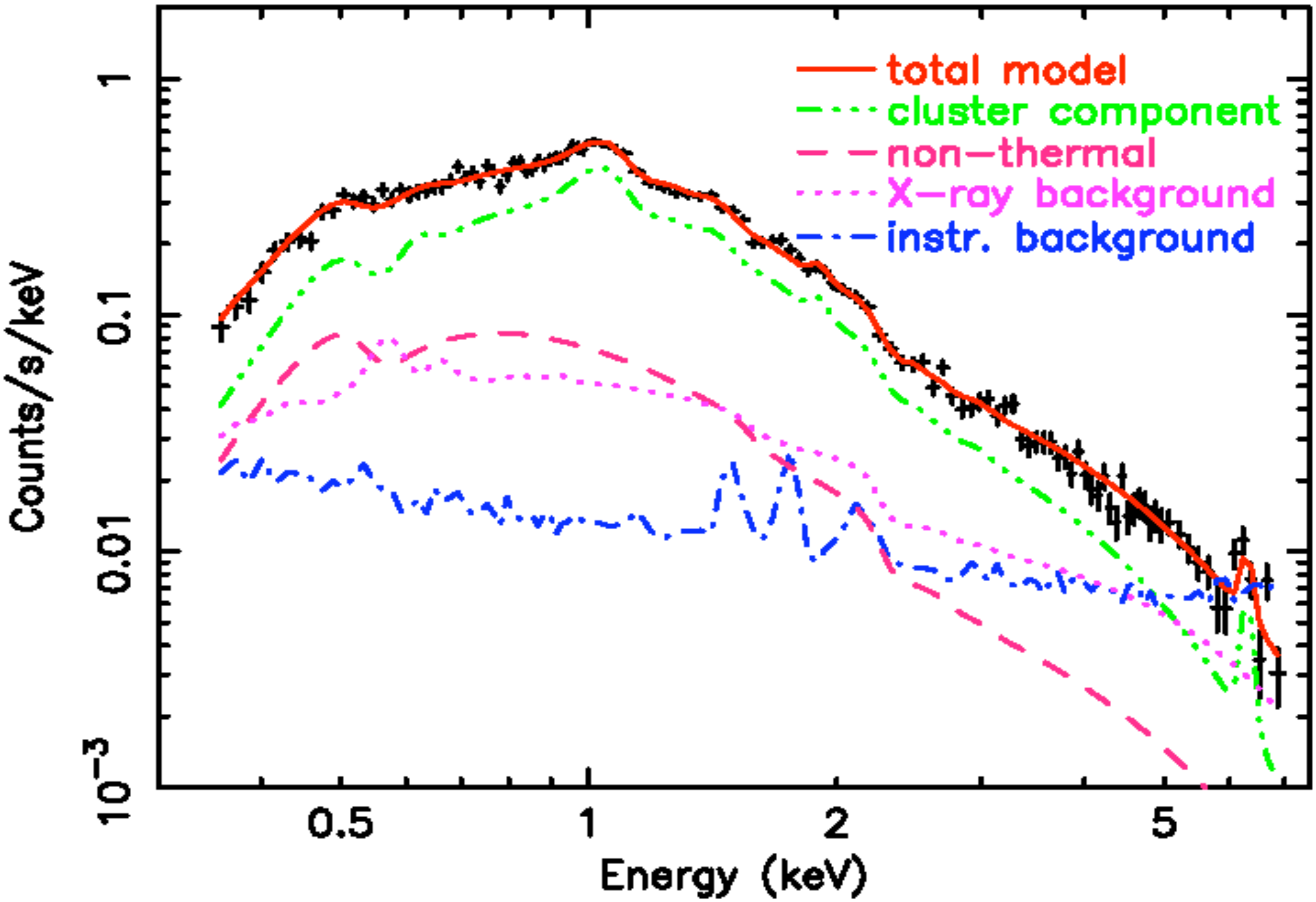

CLUSTER SOFT EXCESS DIAGNOSTICS

Inside a cluster's core the soft excess of clusters is likely to be non-thermal in its nature, due to problems with rapidly cooling of the thermal baryons, and absence of the OVII line.

The soft excess outside clusters' cores might still be of thermal origin.

However, the importance of good background subtraction cannot be overstated – depending on what assumptions you take the potential background can vary by a lot.

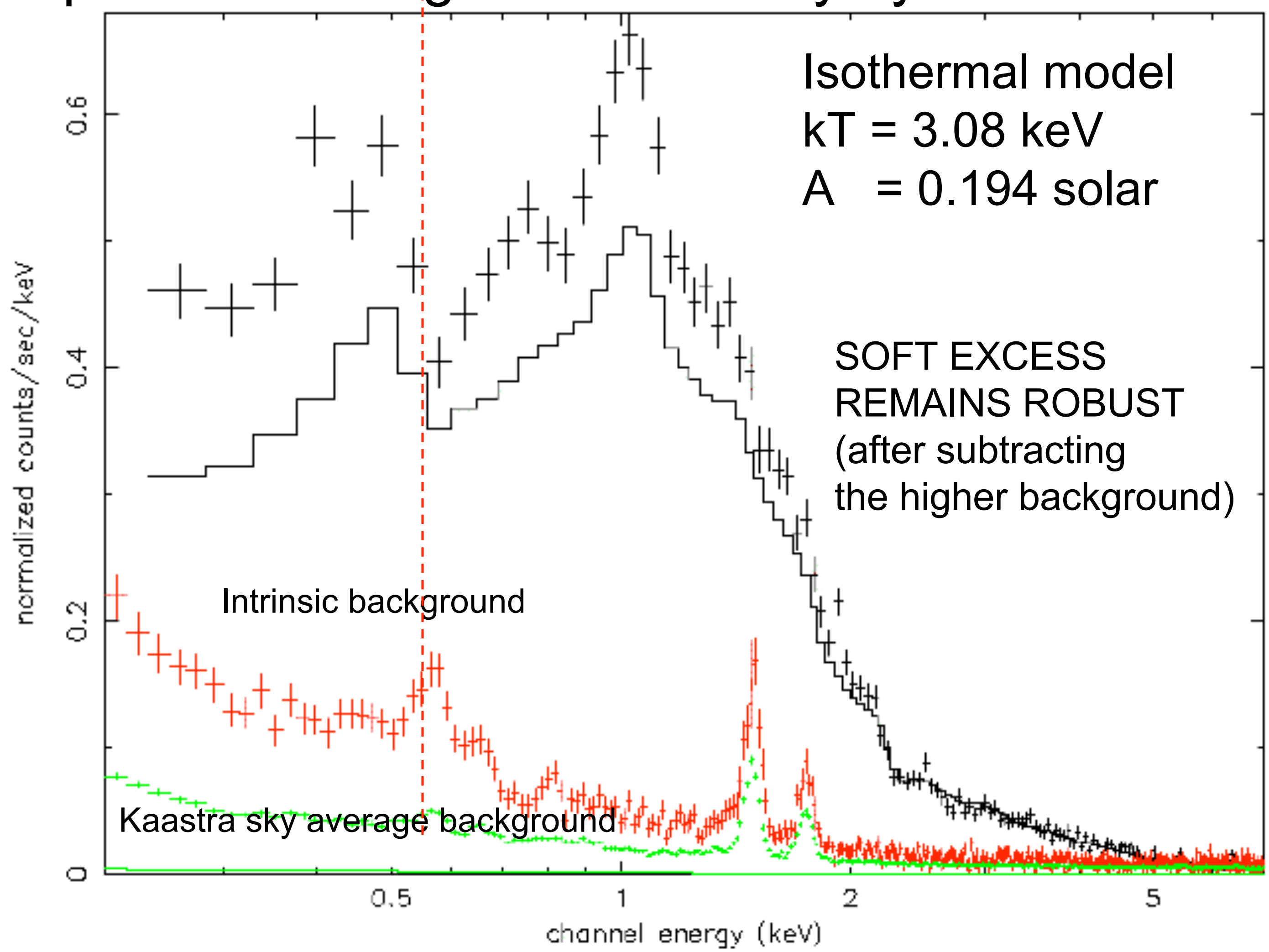

AS1101 (2’-5’) with ICM model (fitted from 2-7 keV) and backgrounds

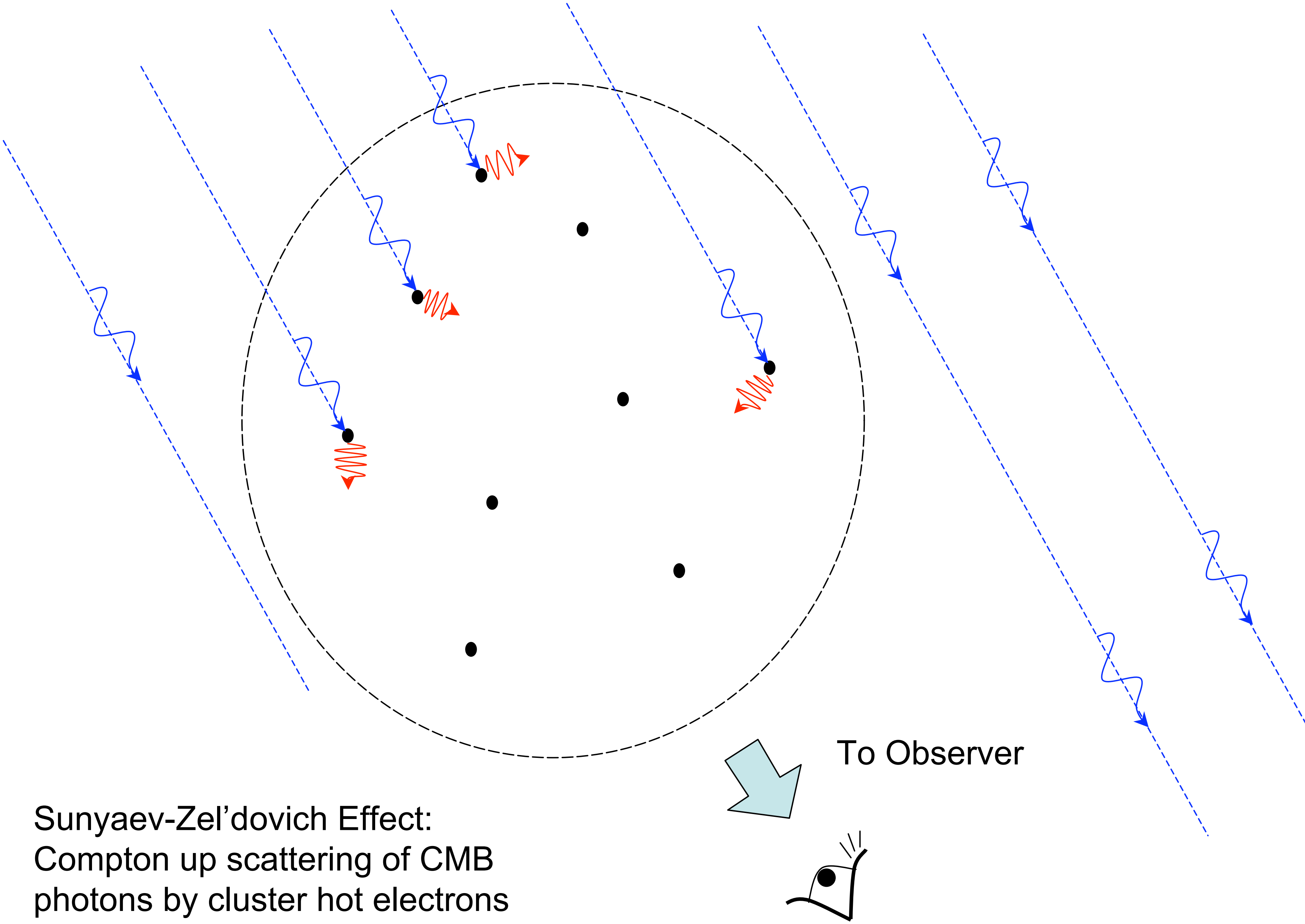

Sunyaev-Zel'dovich Effect:
Compton up scattering of CMB
photons by cluster hot electrons

Basics of the Sunyaev-Zeldovich Effect

$$\frac{\Delta T(\theta)}{T_{CMB}} = -\frac{kT}{m_e c^2}\sigma_T \int dl\, n_e \left[\frac{x(e^x+1)}{e^x-1} - 4\right]$$

The electron density of the hot gas is obtained by fitting ROSAT X-ray surface brightness profiles $I_X(\theta)$ with the 2 parameter <u>isothermal</u> β -model ignoring the central cooling flow

$$n_e(r) = n_0\left[1+\left(\frac{r}{r_e}\right)^2\right]^{-3\beta/2} \Rightarrow I_X(\theta) \propto n_0^2\left[1+\left(\frac{\theta}{\theta_C}\right)^2\right]^{-3\beta+\frac{1}{2}}$$

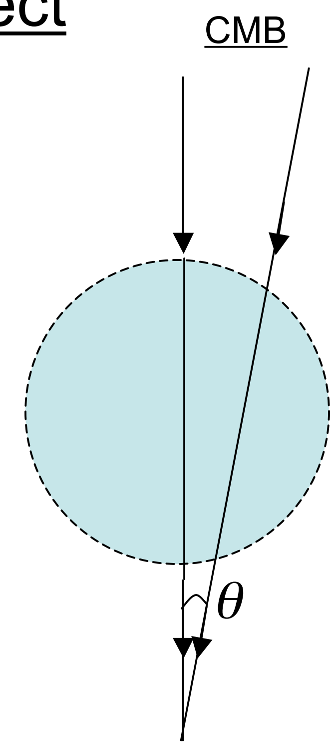

The decrement in T_{CMB} is then given by

$$\Delta T_{SZ}(\theta) = \Delta T_{SZ}(0)\left[1+\left(\frac{\theta}{\theta_C}\right)^2\right]^{-\frac{3\beta}{2}+\frac{1}{2}} \text{ where } \Delta T_{SZ}(0) = -38.8\mu K\left(\frac{n}{10^{-3}\,cm^{-3}}\right)\left(\frac{kT}{keV}\right)\left(\frac{r_C}{Mpc}\right)\left[\frac{j(x)}{-2}\right]\frac{\Gamma\left(\frac{3\beta}{2}-\frac{1}{2}\right)}{\Gamma\left(\frac{3\beta}{2}\right)}$$

with $j(x) = \frac{x(e^x+1)}{e^x-1} - 4$

Name	Galactic (2000)		Redshift	kT	n_0	β	R_{core}	$\Delta T0_Q$	$\Delta T0_V$	$\Delta T0_W$
	Long.	Lat.		(keV)	$\times 10^{-3}$ cm^{-3}		(arcmin)	mK	mK	mK
Abell 85	115.053	-72.064	0.055	7.0	$14.64^{+0.33}_{-0.34}$	$0.58^{+0.03}_{-0.03}$	$1.7^{+0.6}_{-0.8}$	$-0.92^{+0.43}_{-0.32}$	$-0.87^{+0.40}_{-0.30}$	$-0.75^{+0.35}_{-0.26}$
Abell 133	149.761	-84.233	0.057	5.0	$2.98^{+0.13}_{-0.11}$	$0.72^{+0.09}_{-0.07}$	$3.4^{+0.8}_{-0.8}$	$-0.19^{+0.05}_{-0.06}$	$-0.18^{+0.05}_{-0.05}$	$-0.16^{+0.04}_{-0.05}$
Abell 665	149.735	34.673	0.1816	7.0	$3.19^{+0.19}_{-0.22}$	$0.64^{+0.10}_{-0.10}$	$1.3^{+0.1}_{-0.1}$	$-0.38^{+0.08}_{-0.14}$	$-0.36^{+0.07}_{-0.13}$	$-0.31^{+0.06}_{-0.11}$
Abell 1068	179.100	60.130	0.139	5.0	$7.80^{+0.46}_{-0.42}$	$0.90^{+0.17}_{-0.13}$	$1.6^{+0.5}_{-0.5}$	$-0.41^{+0.15}_{-0.15}$	$-0.39^{+0.14}_{-0.14}$	$-0.33^{+0.12}_{-0.12}$
Abell 1302	134.668	48.904	0.116	4.8	$2.88^{+0.19}_{-0.15}$	$0.64^{+0.12}_{-0.08}$	$1.4^{+0.4}_{-0.3}$	$-0.17^{+0.05}_{-0.07}$	$-0.16^{+0.05}_{-0.06}$	$-0.14^{+0.04}_{-0.05}$
Abell 1314	151.828	63.567	0.0341	5.0	$1.00^{+0.27}_{-0.26}$	$0.35^{+0.21}_{-0.10}$	$2.6^{+3.2}_{-2.4}$	$-0.44^{+0.58}_{nan}$	$-0.42^{+0.55}_{nan}$	$-0.36^{+0.47}_{nan}$
Abell 1361	153.292	66.581	0.1167	4.0	$2.34^{+nan}_{-0.61}$	$1.79^{+19.04}_{-1.09}$	$5.2^{+43.8}_{-4.2}$	$-0.16^{+0.18}_{nan}$	$-0.15^{+0.17}_{nan}$	$-0.13^{+0.15}_{nan}$
Abell 1367	234.799	73.030	0.0276	3.5	$1.63^{+0.03}_{-0.03}$	$0.52^{+0.02}_{-0.02}$	$8.6^{+0.5}_{-0.6}$	$-0.16^{+0.02}_{-0.02}$	$-0.15^{+0.02}_{-0.02}$	$-0.13^{+0.01}_{-0.02}$
Abell 1413	226.182	76.787	0.143	6.0	$13.65^{+0.77}_{-0.92}$	$0.68^{+0.11}_{-0.11}$	$1.1^{+0.1}_{-0.1}$	$-0.90^{+0.17}_{-0.29}$	$-0.85^{+0.16}_{-0.27}$	$-0.73^{+0.14}_{-0.24}$
Abell 1689	313.387	61.097	0.181	7.0	$13.79^{+0.75}_{-0.89}$	$0.75^{+0.12}_{-0.12}$	$1.0^{+0.0}_{-0.0}$	$-1.00^{+0.17}_{-0.27}$	$-0.94^{+0.16}_{-0.26}$	$-0.81^{+0.14}_{-0.22}$
Abell 1795	33.788	77.155	0.061	7.0	$3.05^{+0.04}_{-0.06}$	$0.99^{+0.04}_{-0.06}$	$5.2^{+0.3}_{-0.4}$	$-0.33^{+0.03}_{-0.03}$	$-0.32^{+0.03}_{-0.03}$	$-0.27^{+0.02}_{-0.02}$
Abell 1914	67.196	67.453	0.171	9.0	$11.21^{+0.19}_{-0.17}$	$0.85^{+0.04}_{-0.04}$	$1.4^{+0.1}_{-0.1}$	$-1.23^{+0.10}_{-0.10}$	$-1.17^{+0.09}_{-0.10}$	$-1.01^{+0.08}_{-0.09}$
Abell 1991	22.762	60.497	0.0586	4.0	$3.14^{+0.56}_{-0.34}$	$0.82^{+0.54}_{-0.22}$	$2.8^{+2.8}_{-8.4}$	$-0.12^{+0.36}_{-0.13}$	$-0.11^{+0.34}_{-0.13}$	$-0.10^{+0.30}_{-0.11}$
Abell 2029	6.505	50.547	0.0767	9.0	$12.07^{+0.19}_{-0.82}$	$0.67^{+0.03}_{-0.11}$	$1.9^{+0.3}_{-0.3}$	$-1.13^{+0.20}_{-0.40}$	$-1.07^{+0.19}_{-0.37}$	$-0.92^{+0.16}_{-0.32}$
Abell 2142	44.213	48.701	0.09	9.0	$7.17^{+0.41}_{-0.49}$	$0.67^{+0.11}_{-0.11}$	$2.3^{+0.2}_{-0.2}$	$-0.97^{+0.20}_{-0.33}$	$-0.92^{+0.19}_{-0.31}$	$-0.79^{+0.16}_{-0.27}$
Abell 2199	62.897	43.697	0.0302	4.5	$7.35^{+0.11}_{-0.19}$	$0.64^{+0.02}_{-0.04}$	$2.8^{+0.7}_{-1.8}$	$-0.23^{+0.15}_{-0.06}$	$-0.22^{+0.14}_{-0.06}$	$-0.19^{+0.12}_{-0.05}$
Abell 2218	97.745	38.124	0.171	6.0	$2.73^{+0.04}_{-0.18}$	$0.72^{+0.03}_{-0.12}$	$1.5^{+0.1}_{-0.1}$	$-0.25^{+0.02}_{-0.07}$	$-0.24^{+0.02}_{-0.07}$	$-0.20^{+0.02}_{-0.06}$
Abell 2219	72.597	41.472	0.228	7.0	$5.32^{+0.12}_{-0.11}$	$0.78^{+0.05}_{-0.04}$	$1.8^{+0.2}_{-0.1}$	$-0.77^{+0.08}_{-0.09}$	$-0.72^{+0.08}_{-0.08}$	$-0.63^{+0.07}_{-0.07}$
Abell 2241	54.784	36.643	0.0635	3.1	$10.94^{+0.45}_{-0.41}$	$0.74^{+0.09}_{-0.07}$	$1.0^{+0.2}_{-0.2}$	$-0.14^{+0.03}_{-0.03}$	$-0.13^{+0.03}_{-0.03}$	$-0.12^{+0.02}_{-0.03}$
Abell 2255	93.975	34.948	0.08	7.0	$2.25^{+0.05}_{-0.04}$	$0.76^{+0.04}_{-0.04}$	$4.6^{+0.4}_{-0.3}$	$-0.36^{+0.03}_{-0.04}$	$-0.34^{+0.03}_{-0.04}$	$-0.29^{+0.03}_{-0.03}$
Abell 2256	111.096	31.738	0.06	7.0	$3.70^{+0.19}_{-0.23}$	$0.85^{+0.14}_{-0.14}$	$5.5^{+0.9}_{-0.9}$	$-0.48^{+0.10}_{-0.13}$	$-0.45^{+0.10}_{-0.13}$	$-0.39^{+0.09}_{-0.11}$
Abell 2597	65.363	-64.836	0.085	4.0	$14.58^{+0.52}_{-0.68}$	$0.71^{+0.07}_{-0.08}$	$1.4^{+0.6}_{-3.3}$	$-0.45^{+1.10}_{-0.21}$	$-0.43^{+1.04}_{-0.20}$	$-0.37^{+0.90}_{-0.17}$
Abell 2670	81.318	-68.516	0.076	3.0	$3.88^{+0.16}_{-0.16}$	$0.64^{+0.07}_{-0.06}$	$1.9^{+0.7}_{-0.8}$	$-0.13^{+0.06}_{-0.05}$	$-0.12^{+0.05}_{-0.05}$	$-0.11^{+0.05}_{-0.04}$
Abell 2717	349.076	-76.390	0.049	3.0	$8.89^{+0.20}_{-0.18}$	$0.64^{+0.04}_{-0.03}$	$1.5^{+0.2}_{-0.1}$	$-0.16^{+0.02}_{-0.02}$	$-0.15^{+0.02}_{-0.02}$	$-0.13^{+0.02}_{-0.02}$
Abell 2744	8.898	-81.241	0.308	11.0	$3.13^{+0.23}_{-0.17}$	$1.60^{+0.44}_{-0.27}$	$3.3^{+0.6}_{-0.4}$	$-0.87^{+0.19}_{-0.22}$	$-0.82^{+0.18}_{-0.21}$	$-0.71^{+0.15}_{-0.18}$
Abell 3301	242.415	-37.409	0.054	7.0	$4.20^{+0.19}_{-0.18}$	$0.49^{+0.05}_{-0.04}$	$1.8^{+0.5}_{-0.4}$	$-0.38^{+0.11}_{-0.14}$	$-0.36^{+0.10}_{-0.14}$	$-0.31^{+0.09}_{-0.12}$
Abell 3558	311.978	30.738	0.048	5.0	$2.58^{+0.04}_{-0.04}$	$0.78^{+0.04}_{-0.03}$	$5.9^{+0.4}_{-0.4}$	$-0.23^{+0.02}_{-0.02}$	$-0.22^{+0.02}_{-0.02}$	$-0.19^{+0.02}_{-0.02}$
Abell 3560	312.578	28.890	0.04	2.0	$4.62^{+0.22}_{-0.20}$	$0.49^{+0.05}_{-0.04}$	$2.6^{+0.6}_{-0.5}$	$-0.12^{+0.03}_{-0.05}$	$-0.12^{+0.03}_{-0.04}$	$-0.10^{+0.03}_{-0.04}$
Abell 3562	313.308	30.349	0.04	4.5	$6.85^{+0.48}_{-0.60}$	$0.47^{+0.08}_{-0.08}$	$1.3^{+0.1}_{-0.1}$	$-0.25^{+0.08}_{-0.24}$	$-0.23^{+0.07}_{-0.23}$	$-0.20^{+0.06}_{-0.20}$
Abell 3571	316.317	28.545	0.04	7.0	$11.92^{+0.29}_{-0.29}$	$0.65^{+0.04}_{-0.04}$	$3.6^{+0.7}_{-0.8}$	$-0.97^{+0.22}_{-0.21}$	$-0.91^{+0.21}_{-0.20}$	$-0.79^{+0.18}_{-0.17}$
Abell 4059	356.833	-76.061	0.046	4.5	$4.95^{+0.42}_{-0.35}$	$1.00^{+0.29}_{-0.19}$	$6.1^{+2.1}_{-1.8}$	$-0.31^{+0.11}_{-0.13}$	$-0.29^{+0.10}_{-0.12}$	$-0.25^{+0.09}_{-0.11}$
Coma	58.080	87.958	0.023	8.2	$4.38^{+0.24}_{-0.29}$	$0.71^{+0.11}_{-0.11}$	$9.8^{+1.6}_{-1.6}$	$-0.59^{+0.14}_{-0.20}$	$-0.56^{+0.13}_{-0.18}$	$-0.48^{+0.11}_{-0.16}$

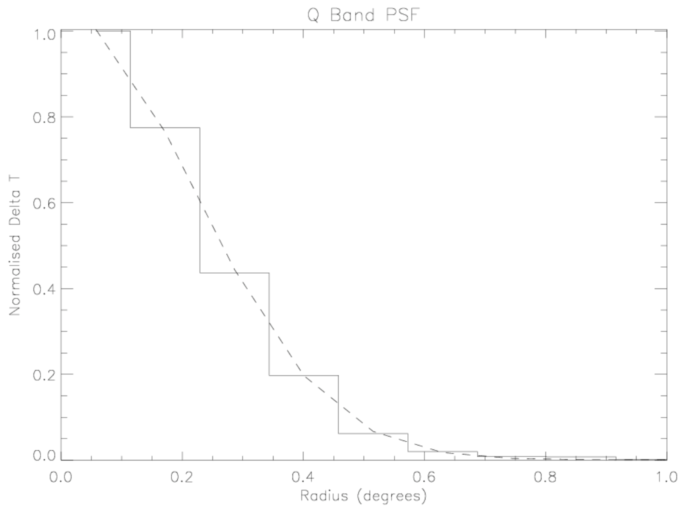
Q Band PSF
Normalised Delta T
Radius (degrees)

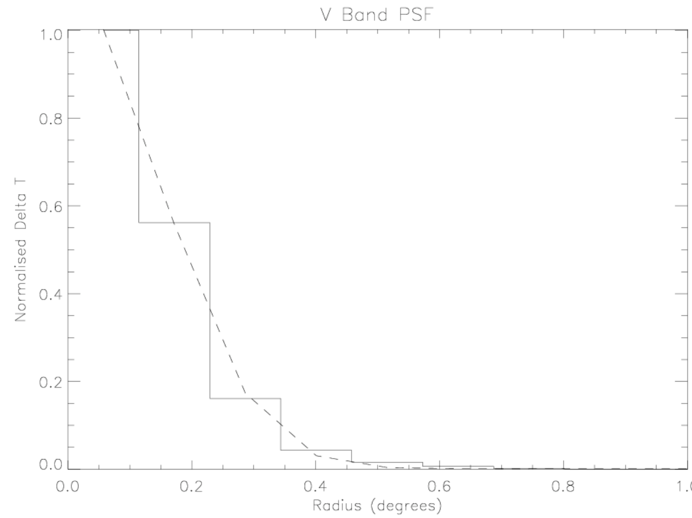
V Band PSF
Normalised Delta T
Radius (degrees)

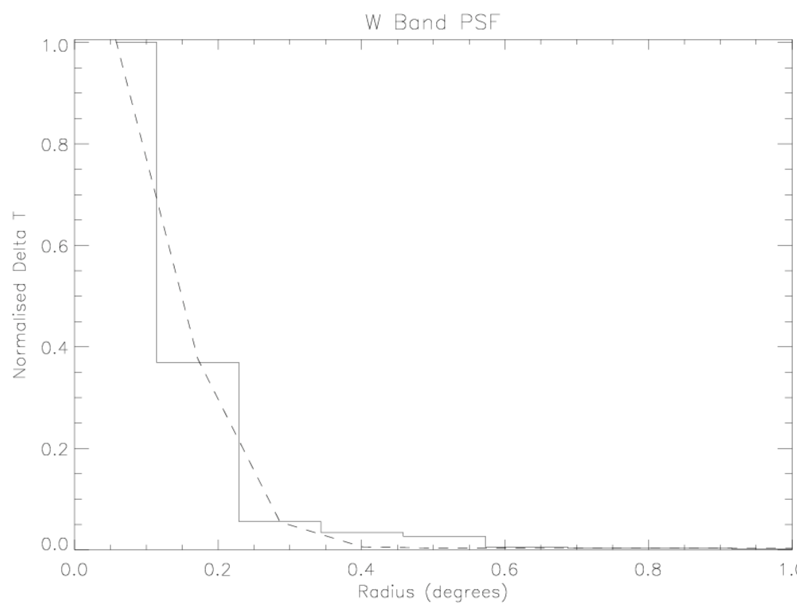
W Band PSF
Normalised Delta T
Radius (degrees)

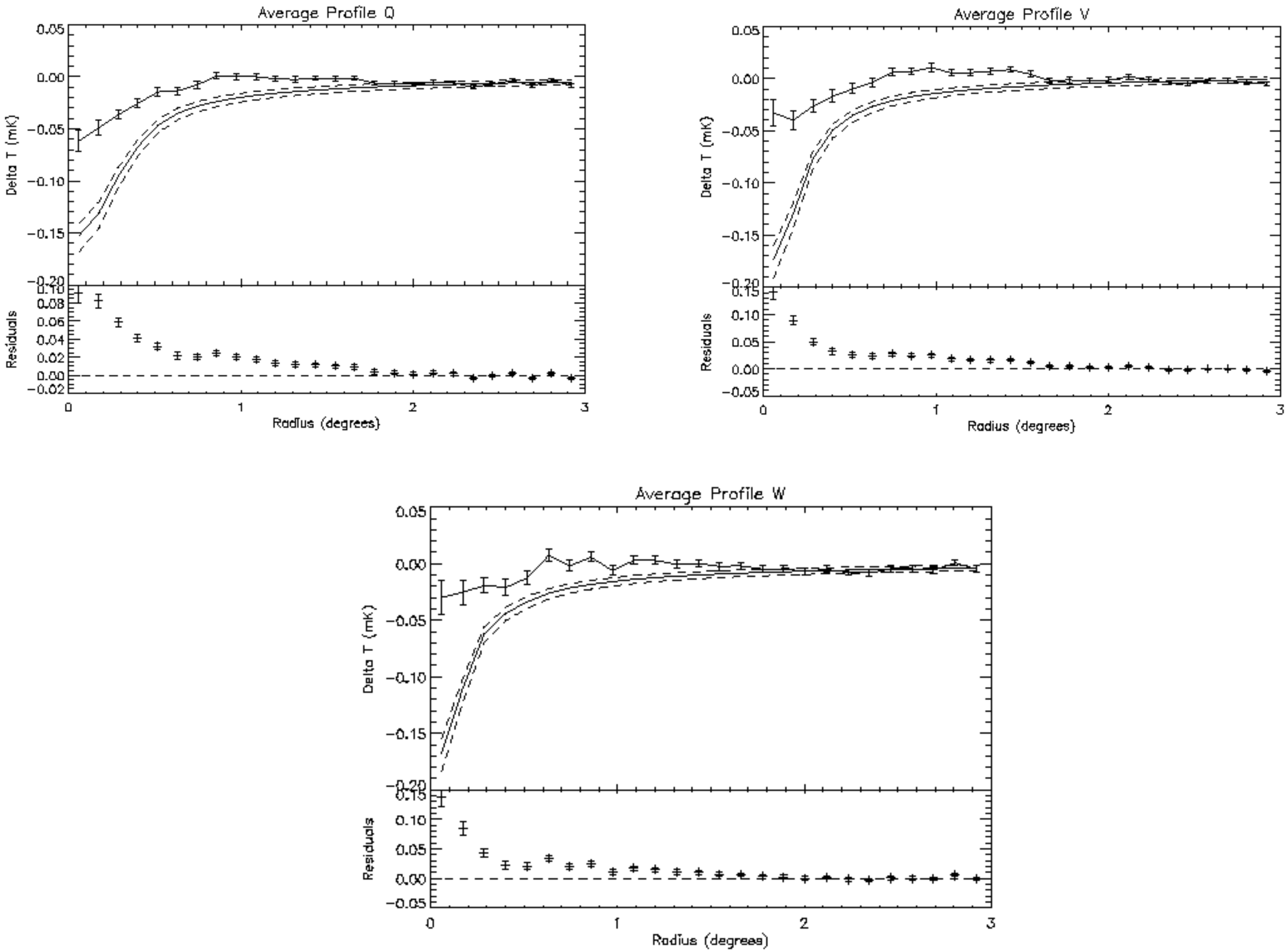

Average Profile Q
Average Profile V
Average Profile W
Delta T (mK)
Residuals
Radius (degrees)
0.05
0.00
-0.05
-0.10
-0.15
-0.20
0.10
0.08
0.06
0.04
0.02
-0.02
0
1
2
3

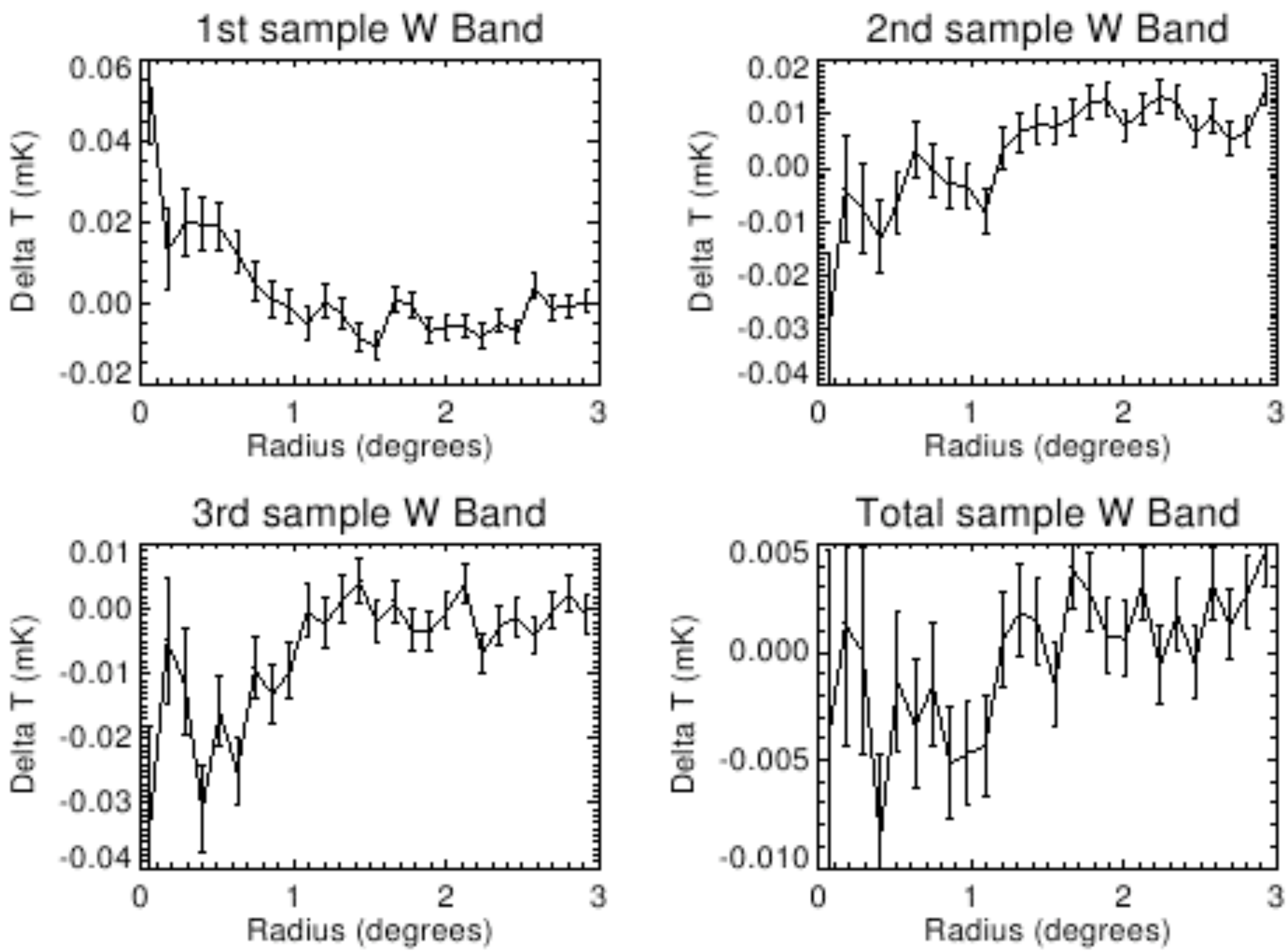
1st sample W Band
Delta T (mK)
Radius (degrees)
0.06
0.04
0.02
0.00
-0.02
0
1
2
3
2nd sample W Band
Delta T (mK)
Radius (degrees)
0.02
0.01
0.00
-0.01
-0.02
-0.03
-0.04
3rd sample W Band
Delta T (mK)
Radius (degrees)
0.01
0.00
-0.01
-0.02
-0.03
-0.04
Total sample W Band
Delta T (mK)
Radius (degrees)
0.005
0.000
-0.005
-0.010

Could cluster radio sources be responsible? The Owens valley radio interferometry survey (Bonamente et al. 2005) shows on average one ~1 mJy source at 30 GHz per cluster. Given their sample is more distant than ours, this would scale to ~ 10mJy or

$$10^{-28}\,\mathrm{Wm^{-2}Hz^{-1}}$$

If this causes our discrepancy it must explain $\delta T_{CMB} \approx 5\times10^{-5}\,\mathrm{K}$ distributed over 0.5 degree.

We can convert δT_{CMB} to flux by multiplying the Rayleigh-Jeans sky flux

$$2\pi k \delta T_{CMB} \nu^2 / c^2$$

by the solid angle $\delta\Omega / 4\pi$ where

$$\delta\Omega = \pi\theta^2$$

with $\theta = 0.5$ degrees. This gives a factor of 10 discrepancy since we get

$$10^{-27}\,\mathrm{Wm^{-2}Hz^{-1}}$$ at $\nu = 30$ GHz (Q Band)

In the W band it is even worse since the spectra goes as $F \sim \nu^{-\alpha}$ where $\alpha \geq 2$ giving a shortfall of at least two orders of magnitude

Bielby & Shanks 2007 MNRAS submitted

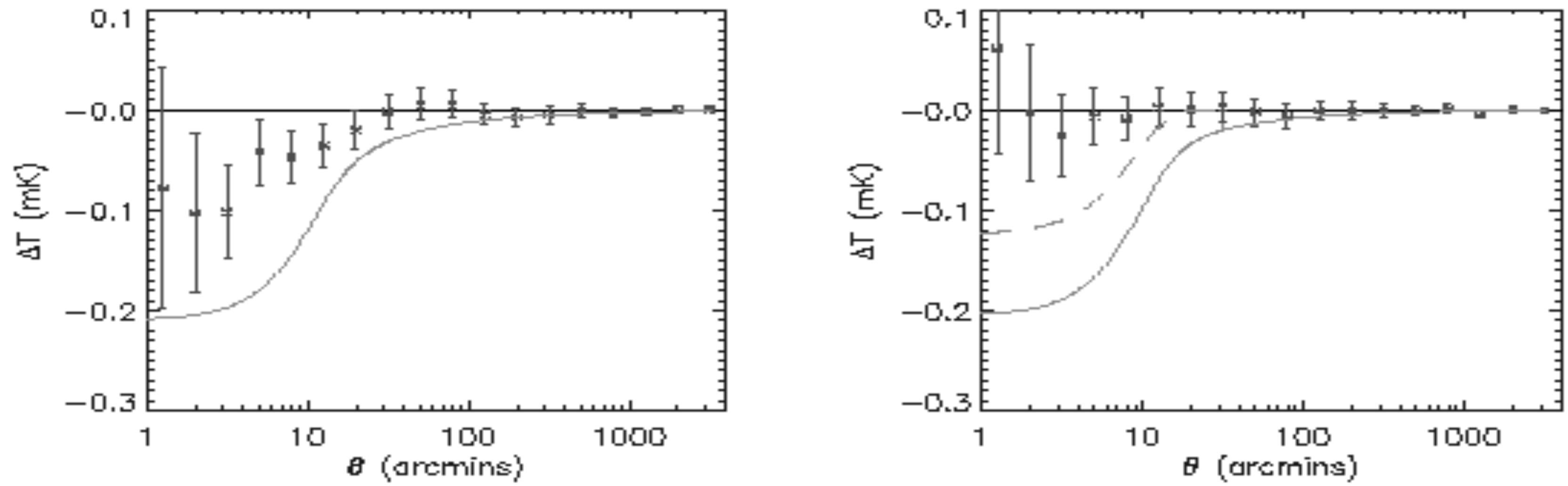

Figure 4. Average ΔT (from WMAP W-band data) plots for 30 clusters from the ROSAT sample (left) and 39 clusters from the Chandra sample (right). In both figures, the points show our cross-correlation results, whilst the curves show average SZ models (based on the parameters taken from Lieu et al. 2006 and Bonamente et al. 2006) convolved with a Gaussian representing the WMAP beam profile. For the Chandra sample, we plot the full isothermal model (solid line) and the same model limited to $\theta < 2'$ (dashed line).

The role of relativistic electrons

- Quenby & Lieu (2006) invoked a power-law population of intracluster relativistic electrons extending to TeV energies.
- In the 0.1-0.5 GeV range they inverse-Compton scatter the CMB to cause soft X-ray excess in clusters.
- The 0.5-3.0 GeV electrons can emit 2-7 keV X-rays by the same IC process, reducing the X-ray gas mass and hence the expected amount of WMAP SZ decrement.
- At 50 GeV energies synchrotron radiation in micro-gauss field occurs at 40 GHz, and also helps to reduce the SZE.
- No violation of the EGRET gamma-ray flux upper limit.
- The relativistic electrons could be the product of extended intracluster Fermi acceleration, or neutralino decay.

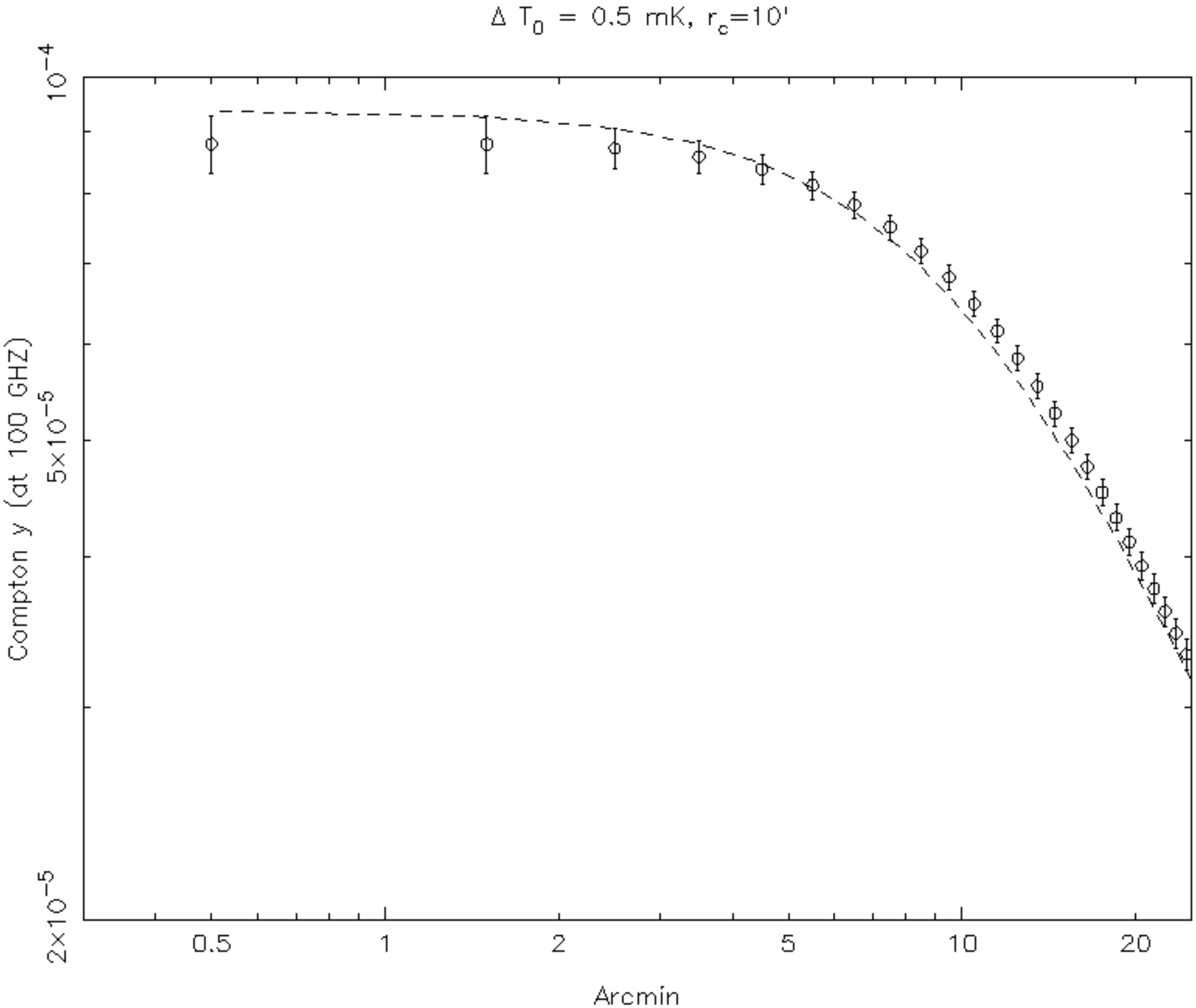

ΔT_0 = 0.5 mK, r_c=10'
Compton y (at 100 GHZ)
10^{-4}
5×10^{-5}
2×10^{-5}
0.5
1
2
5
10
20
Arcmin

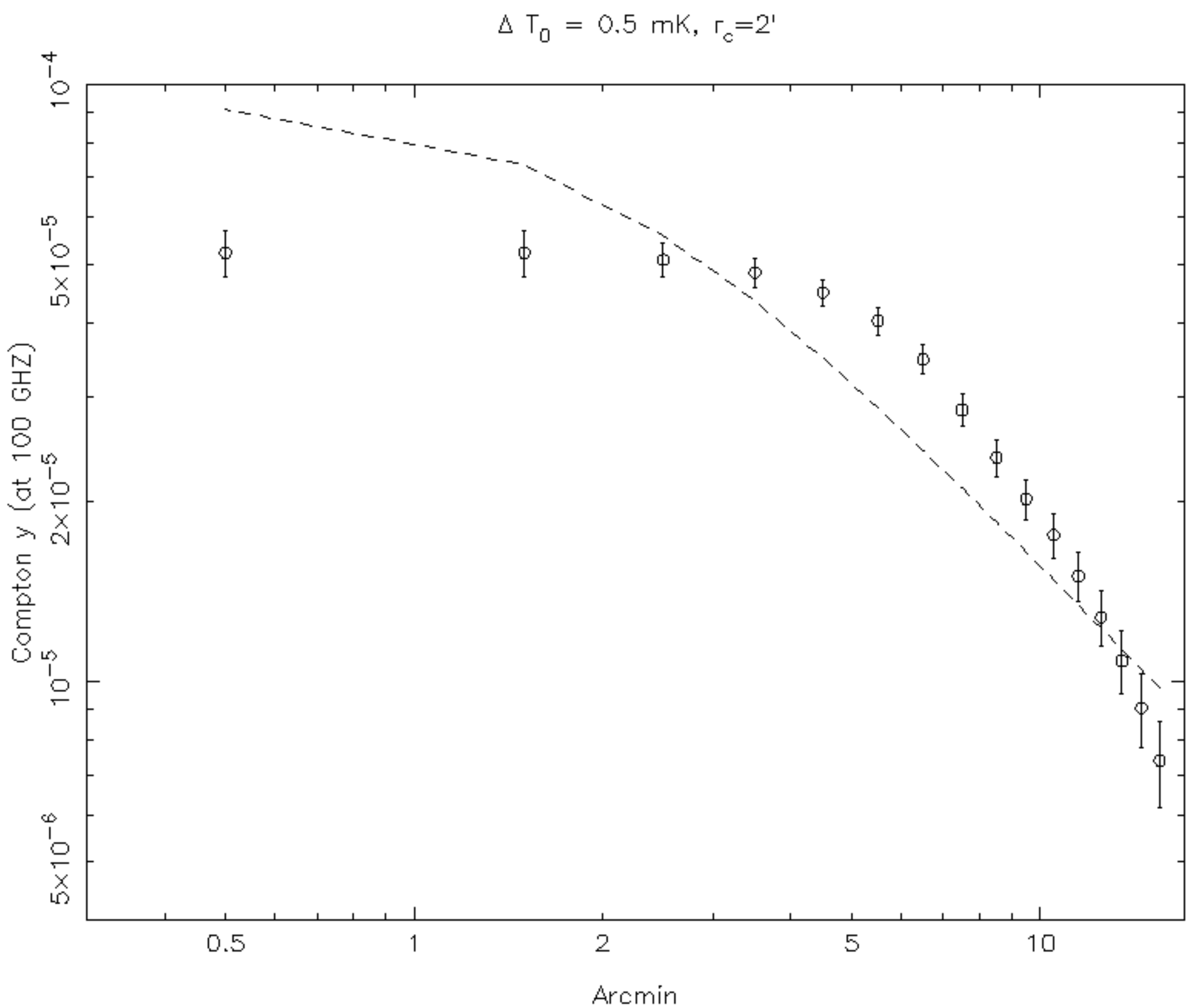

ΔT0 = 0.5 mK, rc=2'
Compton y (at 100 GHZ)
10^-4
5×10^-5
2×10^-5
10^-5
5×10^-6
0.5
1
2
5
10
Arcmin